Nonlinear Analysis of Flow Pulses and Shock Waves in Arteries

Part I: Derivation and Properties of Mathematical Model

By Max Anliker, Robert L. Rockwell[1]), Dept. of Aeronautics and Astronautics, Stanford University, Stanford, California and Eric Ogden, Environmental Biology Division, Ames Research Center, NASA, Moffett Field, California

Notation

A	cross-sectional area of artery at the reference intraluminal pressure p_0
c	local wave speed
c_0, c_1	parameters in wave speed expression
c_L	local wave speed for linearized analysis
C, C'	designations for general curves in z, t plane
D_0	diameter at aortic valve when $p = p_0$
D_t	diameter at distal end of artery when $p = p_0$
E	circumferential Young's modulus
f	axial frictional force per unit mass of fluid
h	wall thickness
L	distance from aortic valve to distal end of artery
n	parameter in wave speed expression
p	intraluminal pressure
$\bar{p}$	calculated mean pressure
p_0	reference pressure
p_c	capillary pressure
p_L	pressure at distal end of artery
q	$S\,v$ = local volume flow rate
q_0	$q_0(t)$ = volume flow rate ejected by heart
r	radial coordinate
R_e	Reynolds number for steady flow
R_L	peripheral resistance
s	curvilinear coordinate
S	cross-sectional area of artery
S_L	cross-sectional area for linearized analysis
t	time
v	axial fluid velocity averaged over cross section
z	axial distance coordinate
z^*	distance from aortic valve to femoral artery
β	exponent in cross-sectional area expression
γ	outflow parameter
λ	undetermined multiplier
μ	blood viscosity coefficient
ϱ	blood density
ψ	outflow function simulating effect of side branches

[1]) Now, Naval Weapons Center, China Lake, California.

I. Introduction

The intermittent ejection of blood from the left ventricle produces pressure and flow pulses in the arterial tree. Experimental studies of these pulses reveal that they are propagated with a characteristic pattern. The pressure and flow pulses are interrelated and constitute a mechanical phenomenon whose features are defined by the physical and geometric properties of the arterial tree. We know from actual measurements on animals and on man that the pressure and flow pulses undergo well-defined changes in their wave form as they propagate away from the heart [1, 2]. These changes have been observed to be quite sensitive to certain variations in the properties of the cardiovascular system. Therefore the question arises, to what extent can deviations of the wave forms from their normal patterns be used as diagnostic indicators or in a study of the control mechanisms responsible for maintaining and regulating blood flow. With the recent development of ultrasound echo-ranging devices and pulsed doppler shift flowmeters which allow us to detect the flow pattern in major arteries without penetrating the skin [3, 4, 5], this question seems to be particularly relevant. However, a meaningful interpretation of changes in the pulse waves is only possible if we have a thorough quantitative understanding of how the various cardiovascular parameters can affect the pressure and flow pulses. As an attempt to develop this quantitative understanding, we have therefore begun a nonlinear analysis of large-amplitude waves in blood vessels which takes into account recently established experimental facts [6, 7, 8].

One of the principal reasons for undertaking the work described in this paper is the need for a noninvasive method of determining possible changes which may occur in the cardiovascular system of astronauts as a result of prolonged exposure to weightlessness [9]. Preventive measures are being contemplated which are designed to inhibit the space adaptation of the circulatory system, and the effectiveness of these measures has to be ascertained in a reliable fashion through transcutaneous measurements. If we succeed in developing noninvasive methods and the necessary instrumentation to quantify essential cardiovascular variables and parameters, it will be possible to better utilize naturally-occurring circulatory phenomena as indicators of health or disease. Moreover, we should then be capable of studying the circulatory control mechanisms in man under truly natural conditions – that is, without trauma and/or anesthesia.

A thorough study of blood flow in arteries or veins presents formidable obstacles. For example, we do not yet know what constitutes a sufficiently accurate mathematical model for the mechanical behavior of the vessel wall and its surroundings. Also, we have yet to establish criteria which indicate when certain simplifying assumptions such as linearity in the system behavior, inviscid flow, one-dimensional flow, etc., can be justified. So far, most theoretical studies of the arterial pressure and flow pulses have been based on linear analyses [1, 2, 10, 11, 12] even though there has been increasing evidence of the presence of strong nonlinear phenomena [6]. Some of the first serious attempts at including nonlinear effects were made by Lambert [13], Streeter et al. [14], Rudinger [12, 15], Barnard et al. [16, 17], and Jones [18], who considered the flow to be one-dimensional and made use of the method of characteristics. The essential advantage of their approach is that the method of charac-

teristics includes automatically the effects of reflections and makes it possible to account for the variations in cross-sectional area with distance and pressure and for the convection of the signal by the flow. Although to-date, no realistic analysis of the generation and evolution of the natural pulse wave in arteries has been made, the referenced investigations have clearly indicated the potential usefulness of the method of characteristics. The availability of faster digital computers and more detailed quantitative information on the mechanical behavior of arteries renders the extension of earlier efforts feasible and timely. Since the theoretical predictions we are aiming for are to be verified and scrutinized in animal laboratories, we have elected to study first the cardiovascular system of the dog without, however, losing sight of ultimate applications to man.

Recent experimental observations [6, 19] on anesthetized dogs suggest that the propagation of large-amplitude pressure waves in arteries or veins is strongly influenced by nonlinear effects. It has been shown that the local phase velocities of artificially induced small sinusoidal pressure signals increase appreciably when we increase the prevailing transmural pressure and flow velocity. At a given transmural pressure, the phase velocities also increase with distance from the heart. Consequently, the natural pressure pulse should exhibit a marked steepening of its wave front with propagation and also an increase in pulse amplitude. Such behavior can be interpreted as being similar to that observed during the initial phases of shock wave formation in a compressible flow field. In the present study we shall examine this similarity and explore the possibility of shock waves evolving from pressure pulses which have large amplitudes and steep wave fronts already at the root of the aorta, such as the pulses encountered with incompetent aortic or tricuspid valves [20, 21, 22][2]).

For sufficiently small pressure perturbations, such as the sinusoidal wavetrains shown in Figure 1, a linearized analysis of the transmission characteristics of these trains can be justified. Also, it can be used to demonstrate that the propagation characteristics of artificially induced signals vary with the naturally-occurring pressure and flow fluctuations [6, 19].

Since arteries do not seem to be significantly dispersive for pressure waves, the phase velocity can be approximated by the speed of signals in the form of finite trains of sine waves [6]. This has been corroborated extensively for the canine aorta in the frequency range from 40 to 200 Hz. In our analysis we shall assume that the nondispersive property is valid also for frequencies as low as 1 Hz. In addition, we shall utilize in an approximate manner the pressure dependence of the wave speed shown in Figure 2 for the thoracic segment of the aorta [23].

The system of one-dimensional nonlinear differential equations for the present problem is hyperbolic which means that the occurrence of shock waves must be considered a distinct possibility. As a matter of fact, the idea of shock waves in blood vessels is not new [21]. Their possible occurrence has been postulated at times in the past [11, 12] but has not been considered seriously because under normal conditions

[2]) In patients with aortic insufficiency, i.e., incompetent or leaking aortic valves, there is extensive regurgitation of arterial blood from the aorta back into the left ventricle. Similarly, in patients with severely leaking tricuspid valves we find regurgitation of venous blood from the right ventricle back into the vena cava. In both cases extremely large pressure pulses may be generated by the heart.

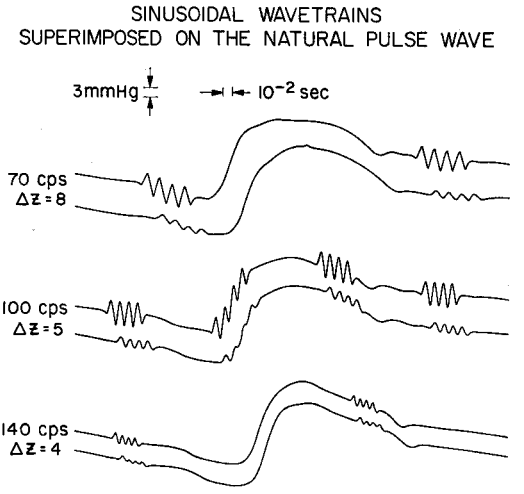

Figure 1
Representative tracings of recordings of the natural pulse wave in the thoracic aorta of an anesthetized dog, with artificially superimposed trains of sinusoidal waves of various frequencies [6]. The transient signals were induced at different times during the cardiac cycle. Note that the sine waves are highly damped but retain their sinusoidal character during propagation. All of the pressure curves are drawn to the same relative scale, as indicated. However, each of the curves has a different zero point since they were separated for illustration purposes. Δz represents the distance between the two catheter-tip manometers used to record the two pressure signals in each pair of curves.

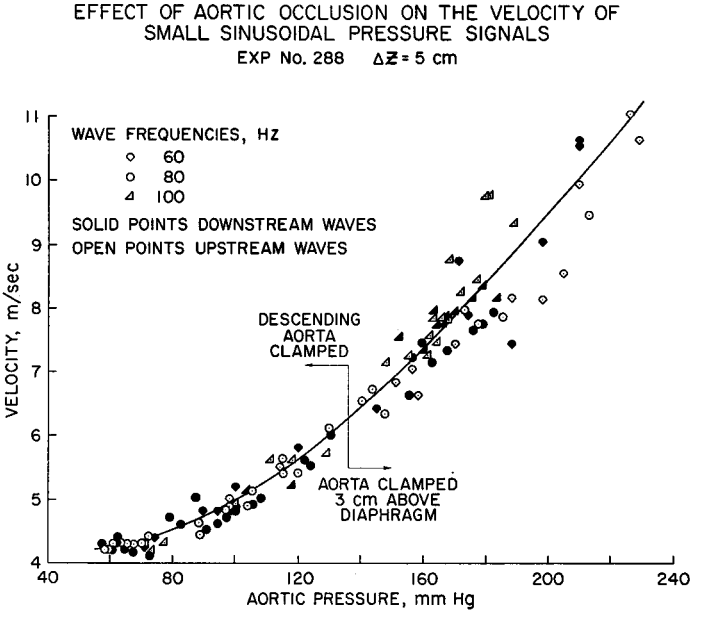

Figure 2
Wave speed-pressure data obtained for thoracic aorta of an anesthetized dog [23]. Each point represents the average speed of a peak and successive valley of a sine wave.

the distances required for their development exceed physiologically meaningful values. However, for very strong pressure pulses with steep wave fronts, the distances at which shock waves can be identified could be within the anatomical range. If we can verify this hypothesis, we could possibly arrive at an explanation for the genesis of the pistol shot sounds which can be heard over arteries in the extremities of patients with incompetent aortic valves [20] or over the corresponding veins in cases of leaking tricuspid valves [22].

In the past, the mechanical properties of the arterial wall were in most cases given in terms of a constant Young's modulus. If we disregard the pressure dependence of this modulus, the wave speed is predicted to decrease with pressure [14], contrary to experimental observations (see Fig. 2). The present study differs insofar as it introduces the mechanical properties of the arterial wall into the equations in a very direct manner through the experimentally observed wave speed as a function of pressure and distance from the heart.

II. Derivations

In this study of large-amplitude wave propagation in arteries, we assume one-dimensional motion of the blood. We model the vessel as a tapered elastic tube and allow for continuously distributed seepage through the wall to simulate the outflow through the branches in a manner which approximates the regional blood flow pattern. The blood is treated as an incompressible fluid and the effects of viscosity are accounted for in an approximate fashion. To define the interaction of the blood with the elastic wall, we prescribe the mechanical behavior of the tube by the speed of small pressure waves and the variation of this speed with pressure and location. With the pressure dependence of the local wave speed, we are stipulating how the cross-sectional area changes when the pressure fluctuations cannot be considered small. The equations governing the fluid flow and the fluid-wall interaction are then transformed according to the method of characteristics and put into a form suitable for machine computation. Such an approach automatically includes reflection phenomena and the essential nonlinearities of the system, and also permits us to obtain solutions corresponding to arbitrary initial conditions and realistic boundary conditions. For the most part, the notation used here is the same as that introduced by Skalak [11] and Rudinger [12] in their survey papers. Although this analysis assumes the cross section of the artery to be circular, it can readily be extended to vessels with non-circular cross sections. By postulating one-dimensional flow, we treat the pressure and flow velocity as uniform over the entire cross section. This is obviously an approximation of reality and means that we are essentially considering spatial average values of the dependent flow variables at each cross section.

1. *Basic Equations*

Conservation of mass requires that the rate of mass increase inside a blood vessel segment of unit length is equal to the net influx of mass. For an incompressible fluid and allowing for outflow of fluid through the arterial wall we have

$$\frac{\partial S}{\partial t} + \frac{\partial (S\,v)}{\partial z} + \psi = 0 \tag{1}$$

where ψ is the rate of volumetric outflow (leakage) per unit length of artery. For the time being, the nature of ψ is left undefined. Its inclusion in the equation simulates the outflow of blood from the artery of interest through discrete bifurcations and branches.

As in Ref. [11] and [12] we write for conservation of momentum

$$\frac{\partial v}{\partial t} + v\frac{\partial v}{\partial z} + \frac{1}{\varrho}\frac{\partial p}{\partial z} = f \tag{2}$$

where f represents the effect of any forces acting on the fluid other than pressure forces. f is a force per unit mass of fluid in the z direction and has the dimensions of an acceleration. Like ψ, it is also temporarily left undefined but will ultimately be restricted to represent only the effects of viscosity.

Since arteries are distensible and tapered, the cross-sectional area varies with pressure and distance z from the heart:

$$S = S(p, z) . \tag{3}$$

We now assume that the functional form of equation (3) is algebraic. It would be quite easy to include an explicit dependence of cross-sectional area on time (such as with respiration or during transient responses to vaso-active drugs). A dependence on velocity could also be incorporated, but there appears to be no need to do so for the normal range of flow velocities in arteries.

Relations (1)–(3) constitute three equations for the three unknowns v, p and S. With the aid of (3) we can write in lieu of (1)

$$S\frac{\partial v}{\partial z} + \left(\frac{\partial S}{\partial p}\right)_z \frac{\partial p}{\partial t} + v\left(\frac{\partial S}{\partial p}\right)_z \frac{\partial p}{\partial z} + v\left(\frac{\partial S}{\partial z}\right)_p + \psi = 0 . \tag{4}$$

Restricting the expressions f and ψ to be algebraic functions of p and v, we have with (2) and (4) a pair of quasi-linear (the coefficients in the equations depend on the unknowns, but not on their derivatives), first-order partial differential equations which we solve by the method of characteristics.

With $\lambda = \lambda(p, v, z, t)$ as an undetermined multiplier, we multiply (4) by λ and add to (2):

$$\left.\begin{aligned} &\frac{\partial v}{\partial t} + (v + \lambda S)\frac{\partial v}{\partial z} + \lambda\left(\frac{\partial S}{\partial p}\right)_z \left[\frac{\partial p}{\partial t} + \left(\frac{1}{\lambda\varrho(\partial S/\partial p)_z} + v\right)\frac{\partial p}{\partial z}\right] \\ &\qquad - f + \lambda v\left(\frac{\partial S}{\partial z}\right)_p + \lambda\psi = 0 . \end{aligned}\right\} \tag{5}$$

For any curve C in the z, t plane, the parametric equations of C can be given in terms of a curve parameter s as

$$z = z(s)$$

and

$$t = t(s) .$$

Along C,

$$\left.\frac{dv}{ds}\right|_c = \left.\frac{\partial v}{\partial t}\frac{dt}{ds}\right|_c + \left.\frac{\partial v}{\partial z}\frac{dz}{ds}\right|_c .$$

We choose C so that

$$\left.\frac{dt}{ds}\right|_c = 1 \quad \text{and} \quad \left.\frac{dz}{ds}\right|_c = v + \lambda S \,. \tag{6}$$

Similarly along another curve C',

$$\left.\frac{dp}{ds}\right|_{c'} = \frac{\partial p}{\partial t}\left.\frac{dt}{ds}\right|_{c'} + \frac{\partial p}{\partial z}\left.\frac{dz}{ds}\right|_{c'}.$$

Selecting C' such that

$$\left.\frac{dt}{ds}\right|_{c'} = 1 \quad \text{and} \quad \left.\frac{dz}{ds}\right|_{c'} = \frac{1}{\lambda \varrho \,(\partial S/\partial p)_z} + v \tag{7}$$

we can reduce (5) to

$$\left.\frac{dv}{ds}\right|_c + \lambda \left(\frac{\partial S}{\partial p}\right)_z \left.\frac{dp}{ds}\right|_{c'} - f + \lambda v \left(\frac{\partial S}{\partial z}\right)_p + \lambda \psi = 0 \,. \tag{8}$$

We now attempt to find a λ for which the curves C and C' coincide, i.e., a λ for which expressions (6) and (7) are identical. This requirement is satisfied if

$$\lambda = \pm \frac{c}{S} \tag{9}$$

where c is defined by

$$c = \sqrt{\frac{S}{\varrho \,(\partial S/\partial p)_z}} \,. \tag{10}$$

Since $dt/ds = 1$ we have $dz/ds = dz/dt$ and the so-called characteristic directions, or base characteristics, are given by

$$\mathrm{I}^{\pm}: \quad \frac{dz}{dt} = v \pm c \,. \tag{11}$$

Inserting (9) and (10) into (8), we obtain the compatibility equations, or characteristic equations:

$$\mathrm{II}^{\pm}: \quad dv \pm \frac{dp}{\varrho c} = \left[f \mp \frac{vc}{S}\left(\frac{\partial S}{\partial z}\right)_p \mp \frac{c}{S}\psi \right] dt \,. \tag{12}$$

The interpretation of these four equations is that II^{+} (equation (12) with the upper signs) is meant to hold on the curve specified by I^{+} (equation (11) with upper sign), and correspondingly II^{-} on I^{-}.

From equation (11), the meaning of c becomes clear: c is the local wave speed, the velocity at which small disturbances are propagated relative to the fluid at rest. For a thin-walled circular cylindrical vessel whose cross-sectional area varies slowly with axial distance, the wave speed expression (10) is equivalent to the classical

Moens-Korteweg relation

$$c = \sqrt{\frac{E\,h}{2\,\varrho\,r}}$$

in which E denotes the circumferential Young's modulus, r the internal radius, and h the wall thickness. Since the solutions for the base characteristics (11) are real, the original system of equations (2) and (4) is hyperbolic.

The solution to the problem can be initiated once the functional form of $S = S(p, z)$ is known. To obtain $S(p, z)$ we could postulate a mathematical model for the mechanical behavior of the arterial wall and then derive the area-pressure relation and the corresponding wave speed expression. However, conventional models for the mechanical behavior of the wall often predict a decrease in wave speed with pressure [14] which, as can be noted from Figure 2, is in contradiction with experimental evidence. This difficulty is automatically avoided if we describe the mechanical behavior of the vessel in terms of the experimentally observed wave speed as a function of pressure and location [23]. The wave speed enters quite naturally into the characteristic equations (11) and (12), and the area-pressure relation can be obtained by integrating equation (10). Finally, by specifying f and ψ together with appropriate initial and boundary conditions, we can arrive at numerical solutions to the problem on hand by integrating equations (11) and (12).

2. *Cross-Sectional Area as a Function of Pressure and Distance*

Measurements in the thoracic aortae of anesthetized dogs [23] suggest that wave speed changes with intraluminal pressure may be approximated by a linear function over the normal physiological range of pressure. Figure 2 displays typical results of wave speed measurements in which the normal range of pressure was extended by appropriate occlusions of the aorta. A quadratic function would approximate the curve in Figure 2 more closely and was in fact used for a number of computer runs. However, the results did not differ significantly from the cases where a linear relationship was employed, and since the amount of computing time required was perhaps 50% greater due to the much more complicated expression for the cross-sectional area corresponding to the quadratic function, we consistently used a linear pressure dependence of the wave speed.

Assuming in addition that the wave speed varies linearly with distance along the aorta [7], we have

$$c(p, z) = (c_0 + c_1\,p)\,(1 + n\,z)\,. \tag{13}$$

By substituting (13) into (10) and integrating the resulting differential equation we find

$$S(p, z) = A(z)\,e^{p - p_0/\varrho\,c(p, z)\,c(p_0, z)} \tag{14}$$

where p_0 is a reference pressure and $A(z)$ is an as yet unspecified function which defines the cross-sectional area of the blood vessel at the pressure p_0 as a function of the distance z from the heart: $A(z) = S(p_0, z)$.

Patel [24] has taken measurements on the major arteries of 11 moderately large dogs with an average weight of 22.1 kg. These measurements are considered as

representative diameters at a given pressure p_0, for example $p_0 = 100$ mm Hg. Assuming a wall thickness-to-radius value of 0.08 in the aorta and one of 0.25 in the external iliac artery, we converted his data to internal diameters corresponding to the pressure p_0 as plotted in Figure 3. However, we are interested in larger animals (the ultimate application is to man), and we have therefore scaled these converted data upward to correspond to a 30 kg dog whose bifurcation was somewhat arbitrarily placed at 54 cm. This was done by increasing the internal diameters obtained from Patel's data by a factor of $\sqrt{30/22.1} = 1.165$, assuming that the ratio of weights is the same as the ratio of lumen areas. The new diameters are also shown in Figure 3.

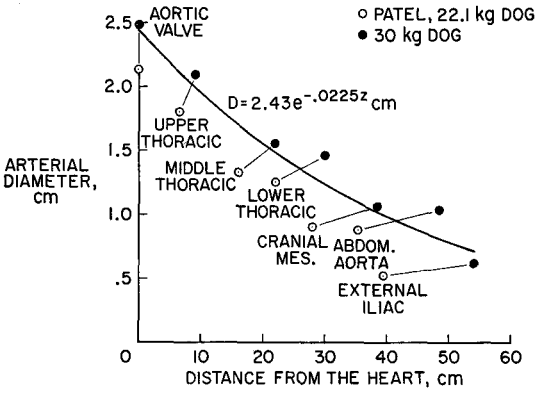

Figure 3
Internal diameter data for the dog aorta according to Patel [24]. The solid curve approximates the diameter variation with distance for the hypothetical 30 kg dog.

An exponentially decreasing diameter appears to be a reasonable approximation for the aorta, according to the data published in the literature and given in Figure 3 (see also Ref. [25]). We therefore could write for $A(z)$:

$$A(z) = S(p_0, z) = S_0(p_0)\, e^{-\beta z} \tag{15}$$

where $S_0(p_0)$ is the cross-sectional area at the root of the aorta at the pressure p_0. With (15) we have

$$S(p, z) = S_0(p_0)\, e^{-\beta z + (p-p_0)/\varrho\, c(p,z)\, c(p_0,z)} \tag{16}$$

and thus a complete definition of the geometry and mechanical behavior of the aorta.

3. *The Friction Expression*

The expression for the force parameter f in equations (2) and (12) will now be restricted specifically to one representing the effects of blood viscosity. As stated before, f must be an algebraic function which unfortunately rules out a more general modeling of the viscous friction which would include proper phase relationship to the pressure. We consider two cases: laminar and turbulent steady flow in a pipe. Making use of the corresponding formulae of Poiseuille and Blasius, we obtain

$$f_{laminar} = -8\pi \frac{\mu}{\varrho} \frac{v}{S} \tag{17}$$

and

$$f_{turbulent} = -.1360 \left(\frac{\mu}{\varrho}\right)^{1/4} \frac{|v|^{7/4}}{S^{5/8}} \operatorname{sgn} v \tag{18}$$

with μ representing the friction coefficient of blood. These expressions are in a strict sense only valid for steady flow but are now assumed to be applicable also for pulsatile flow.

4. *The Outflow Expression* ψ

The outflow of blood from the aorta through discrete side branches and bifurcations is modeled by a continuously distributed leakage or seepage defined by the outflow function ψ. We use the data of Sapirstein [26] on regional blood flow measurements to specify how much blood, in per cent of the total cardiac output, is lost per unit time through the major arteries (identified in Fig. 3 and 4) emanating from the aorta. The results are summarized in Table 1 and Figure 5. It appears that these data are reasonably well approximated by an outflow function which stipulates that the local leakage rate is proportional to the difference $p - p_c$ between the local arterial pressure p and the capillary pressure p_c and which exhibits the gross features of the regional blood flow pattern. Among the various functions considered, the most realistic outflow distribution was obtained with

$$\psi(p, z) = \begin{cases} \gamma\,(p - p_c)\left(1.1 + \cos\dfrac{5\pi}{2}\dfrac{z}{z^*}\right) & \text{for } z \leqslant z^* \\ \gamma\,(p - p_c)\,(1.1)\,e^{-.08(z - z^*)} & \text{for } z \geqslant z^* \end{cases} \tag{19}$$

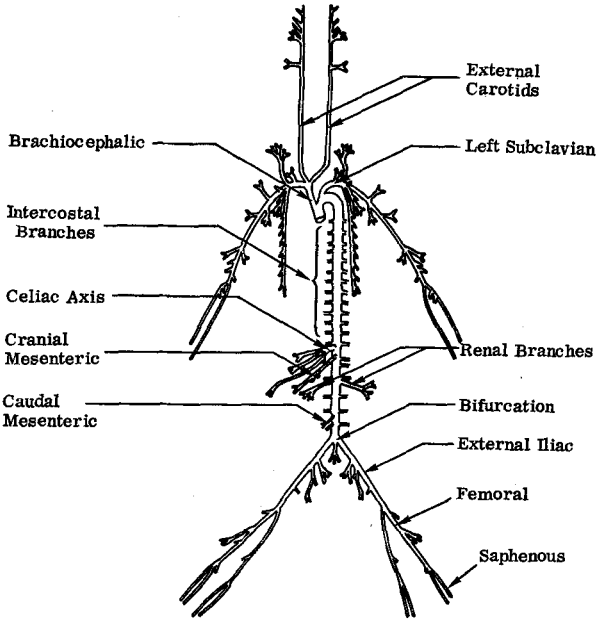

Figure 4
Schematic illustration of the major components of the canine arterial tree, as given in Ref. [27].

Table 1
Approximate distribution of blood through the major arterial branches of the aorta, deduced from Sapirstein's data [26][a]).

Branch	Distance from aortic valve cm	Fraction of cardiac output to branch	Fraction of cardiac output remaining
Aortic valve	0		1.00
Coronary arteries	0+	.05	.95
Brachiocephalic	3	.17	.78
Left subclavian	4	.02	.76
Intercostals, bronchials, diaphragmatic	distributed	.11	.65
Celiac axis	38.5	.08	.57
Cranial mesenteric	40.5	.18	.39
Right renal	42	.06	.33
Left remal	44	.06	.27
Caudal mesenteric	51	.09	.18
Bifurcation	54	.09	.09

[a]) The values given are based in part on Reference [26] and in part on unpublished data collected by Dr. Sapirstein.

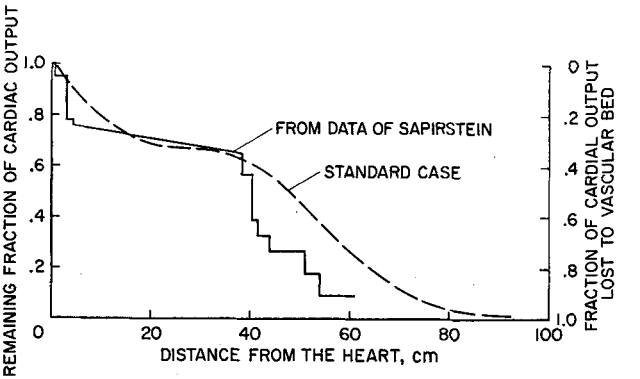

Figure 5
Average distribution of blood plotted from the data of Table 1. The dashed curve is the result of integrating the volume flow rates for the Standard Case (Section III) over a cardiac cycle.

in which z^* represents the distance from the aortic valve to the general region of the femoral artery and $1/\gamma$ is a measure of the outflow resistance. For the cases considered in this analysis z^* was taken to be 70 cm.

The seepage distribution defined by (19) is shown in Figure 6. Near the heart, the outflow is large to simulate the blood flow into the brachiocephalic and left subclavian arteries at the top of the aortic arch. The seepage rate is low in the thoracic region and again large near $z = 50$ cm to approximate the outflow to the abdominal organs and into the bifurcation. The exponential decrease in ψ for $z \geqslant z^*$ accounts for the diminishing outflow into the arteries distal to the femoral region. Since the pressure in the capillaries is of the order of 25 mm Hg, we have chosen this value for p_c in all our computations. The parameter γ was generally chosen such that the diastolic pressure at the heart was of the order of 80 mm Hg.

A typical outflow distribution obtained with this function is given in Figure 5 (Standard Case). It can be seen that the gross behavior of the empirical data is also

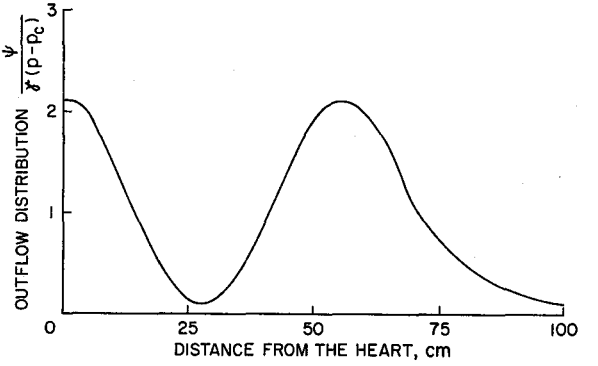

Figure 6
Outflow distribution of blood through the arterial wall as defined by equation (19).

exhibited by the computed results, but the agreement is not altogether satisfactory. This indicates the need for a more appropriate accounting for outflow, although perhaps this effort would be better expended on a model including discrete branches rather than on the purely continuous outflow model considered here. The present procedure for modeling the effect of branches from the aorta is very approximate. However, until more accurate information is available on the true regional flow distribution and its dependence on pressure, approaches such as the one taken here are justifiable.

5. *Boundary Conditions*

The boundary conditions must be specified at the proximal and distal ends of the arterial conduit for which we want to determine the pressure and flow pulse patterns. Each of these boundary conditions can take different forms.

a) Proximal Boundary Condition

There were two types of boundary conditions utilized. The first was to prescribe the variation of the pressure at the aortic valve as a function of time:

$$p(0, t) = p_0(t) .$$

Although this choice seemed a logical one in view of the abundance of actual pressure recordings taken near the aortic valve, it did not give very satisfactory results and was abandoned. The principal disadvantage was that with a representative pressure recording as the proximal boundary condition we could not consistently predict the experimentally observed flow profiles near the aortic valve. The numerical results often exhibited moderate positive and negative flow velocities at the root of the aorta during the latter two-thirds of the cardiac cycle, when the aortic valve is normally closed. (At this stage, we do not wish to deal with incompetent valves.) Clearly, if the true pressure fluctuation were used in conjunction with the actual geometric and elastic parameters, heart rate, cardiac output, outflow function, etc., the predicted flow pulses should be in close agreement with those observed experimentally, provided we have a valid mathematical model for the mechanical behavior of the system. We infer from this that we either do not yet have a sufficiently accurate description

of the mechanical properties of the circulatory system, or that relatively small changes in the pressure pulse produce dramatic changes in the flow pulse and therefore the pressure variation with time must be known to a higher degree of accuracy than we normally have in physiological pressure measurements.

Much more satisfactory results were obtained by specifying the volume flow rate of blood from the left ventricle into the aorta:

$$q(0, t) = q_0(t) .$$

The flow rate is an equally natural choice as a boundary condition. It is related directly to cardiac output and pulse rate both of which can readily be measured and are physically important parameters. Since q is equal to the product of spatial mean flow velocity and cross-sectional area, the boundary condition now takes the form

$$v(0, t) = \frac{q_0(t)}{S(p(0, t), 0)} . \tag{20}$$

In this analysis we shall use the curve shown in Figure 7 [28] as representative of the cardiac ejection $q_0(t)$. Since p and therefore $S(p, 0)$ are not known *a priori*, iteration is necessary to satisfy the boundary condition (20) as stated.

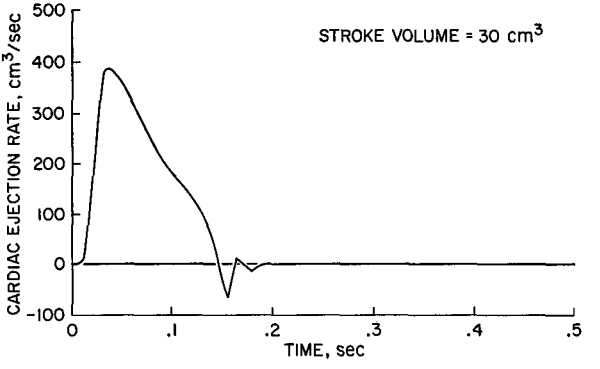

Figure 7
Cardiac ejection rate as a function of time. Adapted from Ref. [28] by scaling to yield a net stroke volume of 30 cm³. As heart rate we have assumed 120 beats per minute.

b) Distal Boundary Condition

As in the case of the proximal boundary we considered two types of conditions at $z = L$. Recognizing that the pulsatile component of blood flow diminishes in the smaller arteries and arterioles and essentially vanishes in most precapillaries and capillaries, we assume that the terminal pressure is constant:

$$p(L, t) = p_L . \tag{21}$$

This is a reasonable approximation only if the diameter at the distal end of the artery is sufficiently small.

The second type of terminal boundary considered is based on the concept of peripheral resistance, which is defined as the ratio of driving pressure across the capillary bed to volume flow rate through this bed. If we take the pressure at the venous end of the capillary as p_c, the driving pressure is $p(L, t) - p_c$. The peripheral

resistance R_L can therefore be expressed as

$$R_L = \frac{p(L, t) - p_c}{q(L, t)} \tag{22}$$

which allows us to write the boundary condition as

$$v(L, t) = \frac{p(L, t) - p_c}{R_L \, S(p(L, t), L)} . \tag{23}$$

The concept of flow rate being proportional to pressure has been widely used in the analysis of blood flow although it seems too simple to be very realistic. Small changes in R_L will usually cause relatively large changes in the pressure and flow along the artery. We decided to choose that value for R_L which produces a representative mean pressure at the heart. The validity of the peripheral resistance idea will be tested by determining the relation between the actual driving pressures and flow rates for specific distances from the heart when a constant end pressure is stipulated as the boundary condition (equation (21)).

6. *Initial Conditions*

From an engineering point of view it might be logical to specify that the velocity everywhere in the arterial conduit is initially zero and that the pressure is at a nominally low level, for example, 25 mm Hg. Then, by initiating the pulsatile ejection of blood from the heart, one can observe the 'starting process'. This could possibly be of some interest in studying the transient response of the cardiovascular system to normal heart beats following a period of cardiac arrest. Similarly, one might want to analyze the response to sudden changes in the system parameters. The initial conditions for that problem would then be the steady state conditions of the unperturbed circulation at the time instant of the occurrence of the change. However, as a rule the initial conditions were usually chosen as close as possible to the anticipated steady state conditions in order to minimize computer time. In assessing the effects of changes in the system parameters, we generally selected as the initial pressure and flow velocity patterns those of the Standard Case (see Section IIIA) at the end of diastole. Of course, the effect of any initial conditions is ultimately damped out and does not influence the steady state solutions.

III. Typical Results – Standard Case

For the most part the IBM 360 computer was used, although some runs were made on the Univac 1108. The so-called method of specified time intervals was employed [14, 29]. The ordinary differential equations (11) and (12) were converted into finite difference equations. Provisions for iteration were included, but with computing intervals of $\Delta z = 2$ cm, $\Delta t = .001$ sec, they proved unnecessary. With this choice, the differences in the computed results were generally less than 1 mm Hg in pressure and 2 cm/sec in velocity when compared with results obtained with much smaller computing intervals. An exception was the case of aortic insufficiency (see Section IVK) in which the large and rapid changes in pressure and flow required intervals of $\Delta z = 1$ cm and $\Delta t = .0001$ sec to maintain the desired accuracy.

Unless indicated otherwise, the following parameter values were used throughout the study:

$\varrho = 1.06$ grams/cm^3,
$\mu = .049$ poise,
$p_0 = 100$ mm Hg $= 1.33 \times 10^5$ dynes/cm^2,
$p_L = 25$ mm Hg $= 3.3 \times 10^4$ dynes/cm^2,
$L = 150$ cm.

The units of pressure used in performing the calculations were usually dynes/cm^2. However, conversion to the more popular millimeters of mercury was generally made for presentation of the results.

To establish a basis of comparison in studying the effects of certain parameters, we defined a Standard Case for the aorta and its continuation beyond the saphenous artery in an anesthetized 30 kg dog. The following physical and geometric features were assumed.

1. Wave Speed:

$$c(p, z) = (97 + 2.03\, p)\,(1 + .02\, z) \text{ cm/sec} \tag{24}$$

where p is the pressure in mm Hg and z is the distance from the aortic valve in cm. This dependence of the wave speed on pressure and distance from the heart approximates the patterns given in the literature [7] and observed in our laboratory [23]. For example, the experimental data shown in Figure 2 represent the wave speed as a function of pressure in the canine thoracic aorta at about 25 cm from the aortic valve.

2. Cross-Sectional Area:

Consistent with equation (16) and the data plotted in Figure 3, we have taken

$$S(p, z) = \begin{cases} 4.63\, e^{-.045z + (p-p_0)/\varrho c(p,z)\, c(p_0,z)} & \text{for } z \leqslant 54 \\ 0.41\, e^{-.089(z-54) + (p-p_0)/\varrho c(p,z)\, c(p_0,z)} & \text{for } z \geqslant 54. \end{cases} \tag{25}$$

The available anatomical data suggest that S varies with z in a different exponential manner for the continuation of the aorta beyond the bifurcation ($z \geqslant 54$ cm) as compared with $z \leqslant 54$ cm. For $z \leqslant 54$ cm we used the data shown in Figure 3, while for $z \geqslant 54$ cm we selected the exponent such that we have a terminal diameter of 100 microns when $L = 150$ cm and $p = p_0$. Originally, a terminal diameter of 10 microns was used, which approximates more closely the capillary size but requires a larger value of L for the same function $S(p, z)$ and thus more extensive computation. However, the results did not differ noticeably and in order to minimize computer time we selected as terminal diameter 100 microns.

3. Heart Parameters and Outflow Expression:

For the Standard Case the pulse rate is 120 beats per minute and the net stroke volume 30 cm^3. This means that the cardiac output of the hypothetical 30 kg dog is 3.6 litters or 0.12 litters per minute per kg mass [30]. The value of γ appearing in equation (19) for the outflow function $\psi(p, z)$ was determined to produce a diastolic pressure of 80 mm Hg. This was achieved for $\gamma = 9.29 \times 10^{-3}$ cm^3/sec/mm Hg.

The pressure and flow velocity profiles predicted for the Standard Case and laminar flow are displayed in Figure 8 for six different locations beginning with $z = 0$ (the aortic valve) and continuing to $z = 100$ cm. Figure 9 shows the temporal mean values for pressure and flow velocity as a function of z together with the diameter at diastolic pressure.

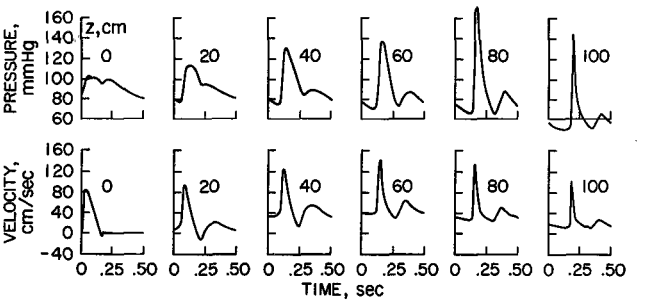

Figure 8
Pressure and flow velocity profiles at six different locations along the artery for the Standard Case. $z = 0$ is the location of the aortic valve. Note steepening of the wave front and peaking of the pulses with propagation. Flow patterns computed at intermediate stations show that flow reversal persists to $z = 30$ cm in this case.

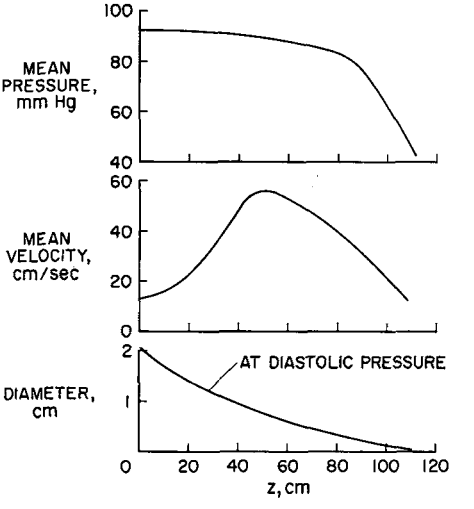

Figure 9
Pressure and flow velocity averaged over the cardiac cycle and plotted as a function of distance from the heart for the Standard Case. Also internal diameter at diastolic pressure.

The temporal pressure profiles plotted in Figure 10 for various distances from the aortic valve indicate the familiar gradual change in shape as the pulse wave propagates in the aorta. We clearly note the incisura in the pressure pattern at $z = 0$. Its sharpness however begins to disappear with increasing distance. In the course of our numerical studies, we observed that the short interval of backflow or negative flow shown in Figure 7 was not necessary to produce the incisura; abrupt decreases in the cardiac ejection rate can cause an incisura even when there is no flow reversal. For the

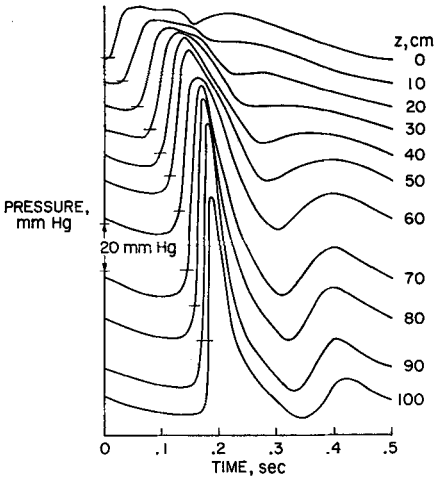

Figure 10
Pressure-time profiles for the Standard Case at different distances from the aortic valve, illustrating the evolution of the natural pressure pulse. The pressure corresponding to 80 mm Hg is denoted at the beginning of each profile.

Standard Case no backflow was found beyond 30 cm. As the pulse wave propagates, the wave front steepens markedly with distance. The pulse pressure grows fastest near $z = 70$ cm and reaches a maximum near $z = 90$ cm. The dicrotic wave first becomes noticeable at $z = 40$ cm and is fully developed past $z = 60$ cm. By integrating the product of area and velocity at each station over a cardiac cycle, we obtain the volume flow at each point. The results are given in Figure 5 for comparison with the empirical data of Ref. [26].

The growth of pulse pressure with increasing distance from the heart correlates well with in vivo observations. That the diastolic pressure decreases with distance has also been noted in experimental studies [2]. However, the variation of the mean flow velocity with distance from the aortic valve as predicted by this analysis has not been mentioned in the literature. In fact, the graphs in Ref. [2] seem to suggest that the mean velocity decreases monotonically with distance. This could be interpreted as an indication of a deficiency in our present model, although the equipment necessary for reliable and accurate measurements of flow velocity in blood vessels has not been generally available.

IV. Basic Properties of Mathematical Model

Having a mathematical model which yields reasonable predictions for the characteristic features of the actual pressure and flow pulses generated by the heart, we intend to study the consequences of making certain basic changes in this model. We are particularly interested in assessing the effects of simplifications which are frequently introduced in elementary theories on blood flow. Whenever we compare the results from any of the altered models with those of the Standard Case, it should be kept in mind that even though the Standard Case solution is used as a reference, it represents an approximation to the pressure and flow pulses observed in reality. However, the computer results discussed are sufficiently accurate to be considered as exact solutions of the mathematical problems defined by the various models.

1. *Semi-Infinite Tubes with Uniform Cross Section*

In order to study the pulse waves in the absence of geometrically induced reflections, we treat the case of a semi-infinite elastic tube of constant diameter. To simplify the problem further, we assume that there is no outflow. For such tubes and various functions $c(p, z)$ we shall examine the flow and pressure pulses induced by a single stroke with an ejection pattern as shown in Figure 7.

The inside diameter of the tube is taken to be 2.43 cm at a pressure of 100 mm Hg. Since there is no geometric taper, the pressure and flow fluctuations should be much lower than those occurring in a moderately tapered tube. Therefore, in order to attain reasonable fluctuations in pressure and flow, we double the stroke volume by doubling the values of cardiac ejection rate given in Figure 7. The initial conditions are zero velocity and a constant pressure of 80 mm Hg everywhere in the tube.

Figures 11 and 12 illustrate the results for four different wave speed functions:

$$c = c(p, z) = (97 + 2.03\,p)\,(1 + .02\,z) \text{ cm/sec} \quad \text{(Standard Case)} \tag{26}$$

$$c = c(z) = (97 + 2.03 \times 100)\,(1 + .02\,z) \quad \text{(independent of } p\text{)} \tag{27}$$

$$c = c(p) = (97 + 2.03\,p) \quad \text{(no variation with distance)} \tag{28}$$

$$c = \text{constant} = (97 + 2.03 \times 100)\,. \tag{29}$$

In all these expressions the pressure p is measured in mm Hg and the distance z in centimeters from the heart. Function (26) exhibits the wave speed variation with pressure and distance as it has been assumed in the Standard Case. Taking in (26) the pressure to be 100 mm Hg, we obtain function (27). Disregarding in (26) the wave

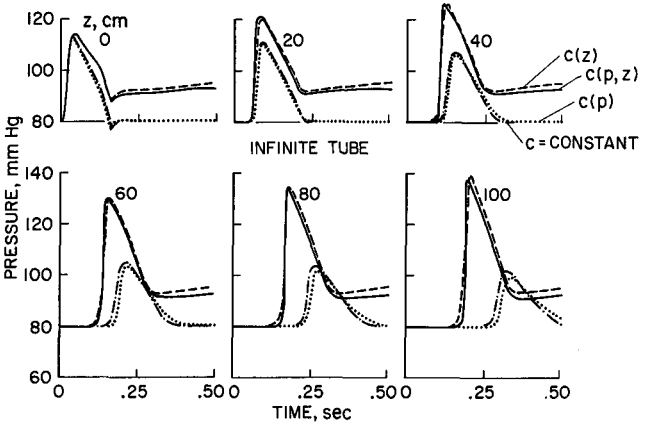

Figure 11

Pressure profiles in semi-infinite tubes with different wave speed functions. The tubes are untapered and there is no outflow through the wall. Ejection pattern is that for Figure 7 but scaled to yield a stroke volume of 60 cm^3. The solid lines represent the results corresponding to $c = c(p, z)$ as defined by expression (26); dashed lines correspond to $c = c(z)$ as given by expression (27). The dotted lines are obtained for $c = c(p)$, and the dash-dot lines illustrate the results for a constant wave speed defined by expressions (28) and (29), respectively.

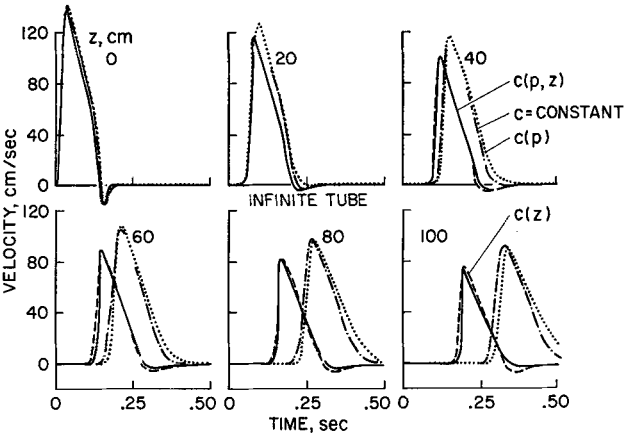

Figure 12
Velocity profiles corresponding to Figure 11 for an elastic tube with constant cross section and different expressions for the wave speed.

speed increase with distance from the heart, we arrive at the expression (28). Finally, both neglecting the spatial variation of the wave speed and assuming an average pressure of 100 mm Hg everywhere, we have the constant wave speed function given by (29).

From Figures 11 and 12 it is clear that the pressure and flow pulses are noticeably changed when we have a wave speed which increases with z. The same observation was also made when we assumed c to be independent of z in the Standard Case. For a meaningful prediction of the natural pressure pulse in the aorta, we must therefore take into account the variation of the wave speed with distance. The influence of pressure dependence of the wave speed appears to be less significant here than is the increase of c with distance. We notice, however, an increase in the slope of the wave front when c is pressure dependent and a more gradual decrease in the pressure or flow for the wave back, as might be anticipated. Since the slopes are already steep, the differences in slope are not readily apparent in the figures but they do in fact amount to factors of two or three.

Functions (26) and (27) stipulate higher wave speeds and thus a stiffer arterial wall than do either (28) or (29). Therefore, with (26) or (27) the pressure pulses arrive at each station sooner and have larger amplitudes than the pulses corresponding to (28) and (29). We also note that for functions (28) and (29), the pressure returns to 80 mm Hg after the ejection ceases, whereas for the cases of the tube becoming stiffer with increasing distance from the origin, the pressure remains elevated for the time periods considered.

For the functions (27) and (29) the individual changes in shape of the pressure and flow pulses with increasing distance from the origin can at least in part be attributed to fluid viscosity. The nonlinear effects due to the wave speed variation with flow velocity, to the local changes in cross-sectional area with pressure, and to the local taper generated by the pressure pulse are still present and also cause modifications of the results.

For the wave speed functions considered there is no evidence of a dicrotic wave in any of the pressure pulses.

2. *Linearized Treatment*

The differential equations (2) and (4) for one-dimensional fluid flow are inherently nonlinear. If we linearize these equations, we reduce the problem to one which can be treated by conventional methods such as Fourier analysis. As a matter of fact, most of the past studies of pulsatile blood flow are based on linearized equations, even though it has been recognized that linearization constitutes an approximation. While such an approximation may be tolerable in analyzing the gross behavior of the system in some cases, it can introduce excessive errors in a prediction of the detailed variations in the pressure and flow patterns with distance from the heart. To determine the magnitudes of these errors in our case, we have set out to examine the differences between the solutions of nonlinear and linear analyses.

If we consider the fluid velocity and the deviation of the pressure from a mean value $\bar{p}$ as perturbations, the linear approximations to the governing differential equations (2) and (4) can be written as

$$\frac{\partial v}{\partial t} + \frac{1}{\varrho}\frac{\partial p}{\partial z} = f(\bar{p}, v, z) \tag{30}$$

and

$$S_L(\bar{p}, z)\frac{\partial v}{\partial z} + \left(\frac{\partial S_L}{\partial p}\right)_z\Big|_{p=\bar{p}}\frac{\partial p}{\partial t} + v\left(\frac{\partial S_L}{\partial z}\right)_p\Big|_{p=\bar{p}} + \psi = 0\,. \tag{31}$$

$S_L(p, z)$ denotes the cross-sectional area relation for the linearized problem. The original outflow expression ψ is linear in the dependent variables and does not have to be modified.

The method of characteristics applied to these equations yields

$$\mathrm{I}^{\pm}: \quad \frac{dz}{dt} = \pm c_L \tag{32}$$

and

$$\mathrm{II}^{\pm}: \quad dv \pm \frac{dp}{\varrho\, c_L} = \left[f(\bar{p}, v, z) \mp \frac{v\, c_L}{S_L}\left(\frac{\partial S_L}{\partial z}\right)_p\Big|_{p=\bar{p}} \mp \frac{c_L\,\psi}{S_L(\bar{p}, z)}\right] dt \tag{33}$$

where the wave speed is now independent of pressure.

$$c_L(z) = \sqrt{\frac{S_L(\bar{p}, z)}{\varrho\,(\partial S_L/\partial p)_z|_{p=\bar{p}}}}\,. \tag{34}$$

As before, we prescribe the spatial variation of the wave speed and then integrate equation (34) to determine the dependence of the cross-sectional area on pressure. Specifying the geometric taper again by (15) we obtain

$$S_L(p, z) = S_0(p_0)\, e^{-\beta z + (p-p_0)/\varrho\, c_L^2}\,. \tag{35}$$

We note that S_L grows exponentially with pressure, whereas in the nonlinear analyses the cross-sectional area defined by (13) and (16) approaches an upper limit with $p \to \infty$, namely

$$\lim_{p\to\infty} S(p, z) = S_0(p_0)\, e^{-\beta z + 1/\varrho\, c_1 (1 + n z) c(p_0, z)}\,.$$

Especially relevant would be a comparison of linear and nonlinear analyses for the Standard Case. We choose the mean pressure of the nonlinear solution as the pressure $\bar{p}$, about which the linearization is made. Accordingly, we take $\bar{p} = 88$ mm Hg. For the wave speed expression, we use equation (24) with the pressure set identically equal to 88 mm Hg.

Figures 13 and 14 illustrate the solution of both the linear and nonlinear problems. In the linearized case, the systolic pressure is higher in the proximal aorta than predicted by the nonlinear treatment because the increase in cross-sectional area with pressure (distension) is no longer present as a pressure-alleviating phenomenon. As z increases, the difference between the systolic pressures diminishes and changes sign. This may in part be due to the fact that the outflow from the proximal aorta is higher for the linear analysis than for the nonlinear one. (The outflow is proportional to the pressure.) Therefore, a smaller flow pulse reaches the distal portions of the artery in the linear case, giving rise to a smaller pressure pulse there.

In the linear case, the wave fronts are considerably less steep and do not increase their slopes appreciably with distance. The wave backs are steeper so that the wave peaks are delayed, but the valleys occur at approximately the same time. As the pressure increases above the average value $\bar{p}$, the arterial wall becomes stiffer in the nonlinear analysis causing a progressive steepening of the wave front; conversely, as the pressure falls below the average value, the vessel becomes more distensible which in turn produces more moderate slopes. These differences become more pronounced with increasing distance from the heart. It is evident that the slope does not vary

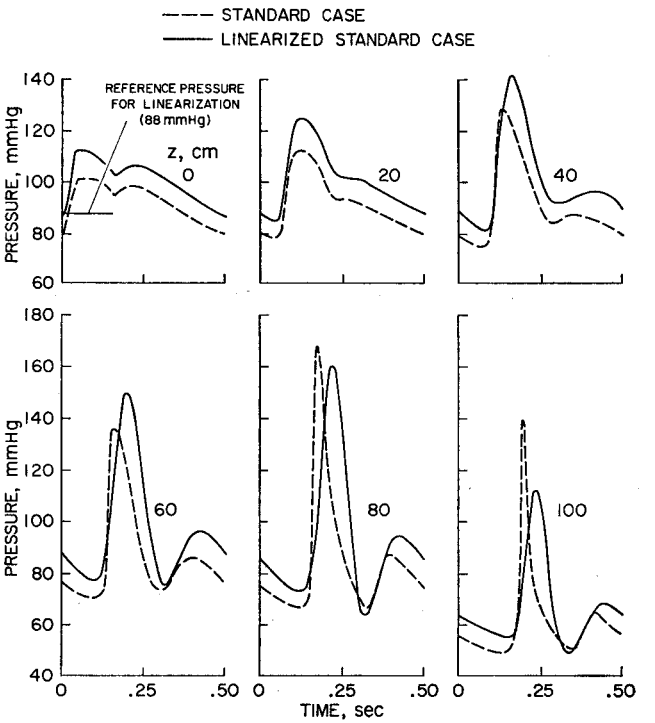

Figure 13
Pressure patterns corresponding to the Standard Case in which nonlinear effects have been taken into account, and patterns computed from the linearized equations. Aside from the mean pressure, the differences in shape become more pronounced with increasing distance from the heart.

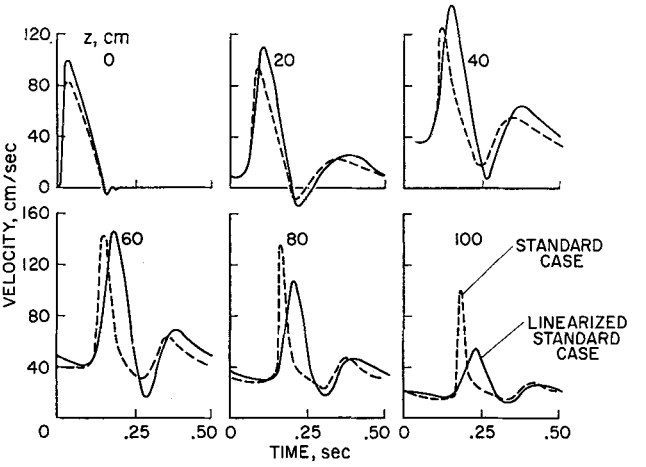

Figure 14
Velocity patterns for the Standard Case computed on the basis of nonlinear and linear analyses. The corresponding pressure patterns are shown in Figure 13.

appreciably between the bottom and top of each pulse in the linear solution. Also, the rate of pressure rise at the front of the pulse is approximately equal to the rate of decay at the back.

We also note that the dicrotic wave is larger in the linear approximation. One possible explanation for this could be the increased stiffness of the distal portion of the artery in the linear case which was introduced by selecting $\bar{p} = 88$ mm Hg for all z. Since the dicrotic wave appears to be caused by the reflection of the primary pressure pulse from the distal portions of the artery, it can be expected that the larger dicrotic wave is due to a stiffer distal end, i.e., a harder reflection region in the linear analysis.

The prominent differences seen between the two solutions indicate that a reliable interpretation of the possible causes for relatively small changes in the naturally occurring pressure and flow pulses can be made only if nonlinear phenomena are taken into account.

3. *Effect of Friction*

There is evidence that fluid friction does not play a dominant role in the large arteries [31] but becomes increasingly important when we approach the capillary bed. The results discussed so far are all based on a friction coefficient corresponding to steady laminar flow. In order to assess to some degree the importance of frictional effects, different values of the viscosity coefficient μ were assumed and the results compared with the Standard Case. It has been stated [32] that the 'effective' viscosity coefficient for pulsatile flow in the large arteries is of the order of eight times that associated with steady flow. Therefore, the effect of increasing μ ten-fold as compared with the Standard Case was examined. In addition, the inviscid approximation was investigated. An increase in the viscosity coefficient produces a higher flow resistance and therefore a decrease in the flow velocity and an increase in the pressure, at least in the proximal aorta. The inviscid case should essentially yield opposite results. With the retarding effects of friction removed, the flow velocity pulse, and correspondingly the pressure pulse, should have a larger magnitude for smaller diameters.

The results plotted in Figures 15 and 16 confirm these expectations. For the larger viscosity coefficient, the overall pressures are higher when $z < 40$ cm and the pulse

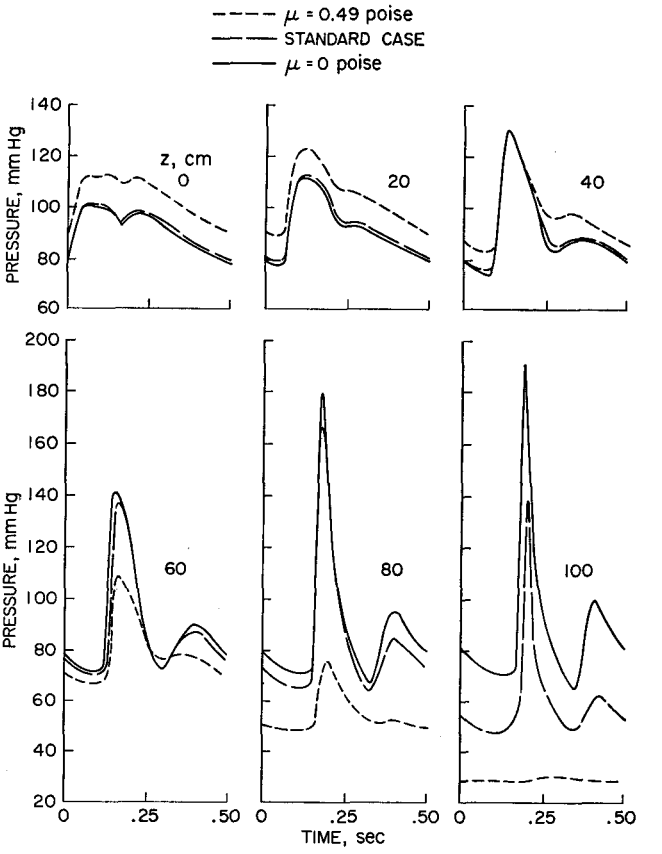

Figure 15
Pressure-time profiles for different values of effective viscosity coefficient in the laminar model for the friction term. The Standard Case (μ = .049 poise) is shown for comparison.

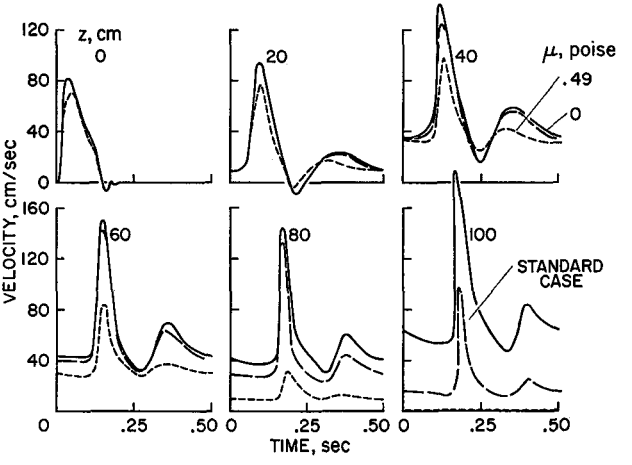

Figure 16
Velocity-time profiles for different values of viscosity coefficient corresponding to the pressure profiles shown in Figure 15.

pressure at the heart has increased slightly. The resistance to outflow along the artery should actually be greater for a more viscous fluid, but this detail was not included in the model for the outflow function ψ. Its proper inclusion would tend to increase the pressures further. Beyond 40 cm, the cumulative effects of increased friction cause such a rapid decay of the pressure and velocity pulses that they are virtually damped out at 100 cm from the heart. In a relative sense, the amplitude of the dicrotic wave has been reduced more markedly than that of the primary pulse. One possible explanation for this can readily be given. If the dicrotic wave is indeed caused by reflection, it must exhibit the effects of friction in a compounded fashion.

The case for $\mu = 0$ is not quite a true inviscid solution because the terminal pressure, left unchanged at 25 mm Hg, would undoubtedly be different for $\mu = 0$. While a true inviscid formulation would lead to an altered terminal condition, the investigation of that problem would not be of practical interest. Our intention here is to approximate reality as closely as possible, and we have therefore left the distal boundary condition unchanged.

For the larger viscosity coefficient of $\mu = .49$ poise, the pressure and flow pulses are significantly different from those of the other cases ($\mu = 0, .049$). If the 'effective' viscosity coefficient is in fact of this order of magnitude, then fluid viscosity does play an important role, even in arteries as large as the aorta. On the other hand, the comparison of the case $\mu = 0$ with the Standard Case suggests that the differences due to friction are not great for $z \leqslant 60$ cm where the mean diameter is larger than 0.6 cm. Beyond that region, the pressure and velocity fluctuations for $\mu = 0$ progressively depart from those of the Standard Case.

Aside from the laminar Poiseuille expression (17), the Blasius formula for steady turbulent flow in a pipe was also used for the cases $\mu = .049$ poise and $\mu = .49$ poise. As can be noted from Figures 17 and 18, the pressure and flow pulses are remarkably unaffected by turbulent friction, especially for $z < 80$ cm. Deviations are observed only for $z \geqslant 80$ cm or for diameters less than 0.3 cm where the flow is unlikely to be turbulent. Only near the heart is turbulent flow normally considered possible. The differences between results for the two values of μ are not profound because the tur-

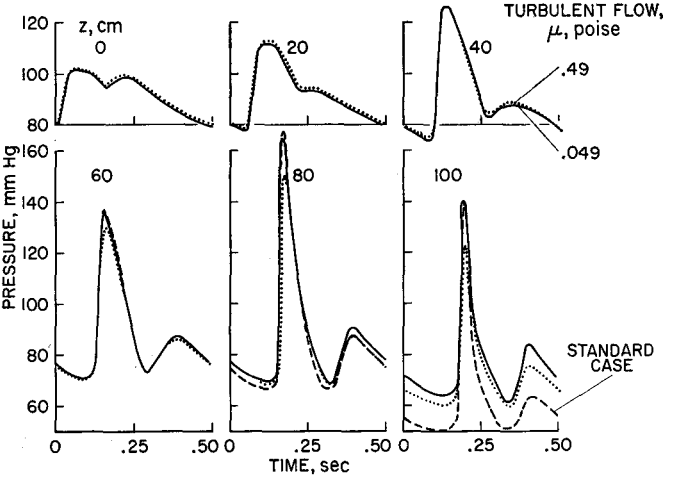

Figure 17
Changes in the pressure patterns resulting from different values of effective viscosity coefficient in the turbulent model for fluid friction. The Standard Case (laminar flow, $\mu = .049$ poise) is also shown.

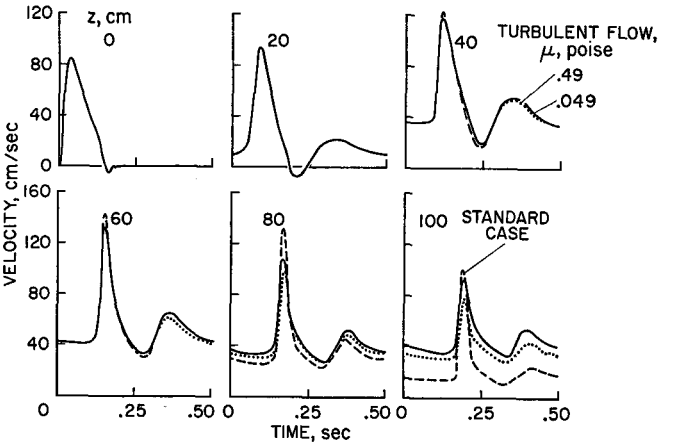

Figure 18
Velocity patterns for turbulent friction corresponding to pressure patterns shown in Figure 17.

bulent expression for friction (18) includes the coefficient of viscosity raised only to the one-fourth power.

Since we are dealing here with friction models which are in some sense artificial, we can not perform a true investigation into the importance of fluid viscosity. All we can say is that an increase of the viscosity coefficient from 0.049 to 0.49 poise in our laminar frictional term produces considerable changes in the pressure and flow pulse, particularly at larger distances from the heart. By contrast, the same increase in μ does not induce significant changes when the turbulent friction term is utilized. However, it remains to be shown whether the expressions chosen for the frictional term are adequate representations of the true situation. Clearly, a thorough investigation of the effects of fluid viscosity on large-amplitude pulsatile flow in distensible tubes should be conducted.

4. *Peripheral Resistance*

The notion of peripheral resistance is applicable when the pressure and flow pulses are linearly related. The adequacy of such a concept for the distal boundary condition should be investigated. We are doing this by utilizing as the distal boundary condition the fact that the pressure is essentially constant in the vicinity of the capillaries. The corresponding solution for the Standard Case is then examined as to the pressure-flow relationship at various distances from the heart. Figure 19 gives the results in terms of the instantaneous blood velocity as a function of instantaneous pressure at four different distances from the heart. If we can disregard the cross-sectional area changes with pressure, the local blood velocity is directly proportional to the local blood flow. For small diameters, we may indeed neglect the cross-sectional area changes and therefore interpret the curves in Figure 19 as approximations of the pressure-flow relations. We note that with decreasing distance from the heart, the pressure-flow relationship deviates progressively from a linear one.

To further assess the effects of prescribing a peripheral resistance R_L, we have considered the Standard Case artery and suitably selected a value for R_L at each of the various distances z from the heart indicated in Figure 19. This means we have

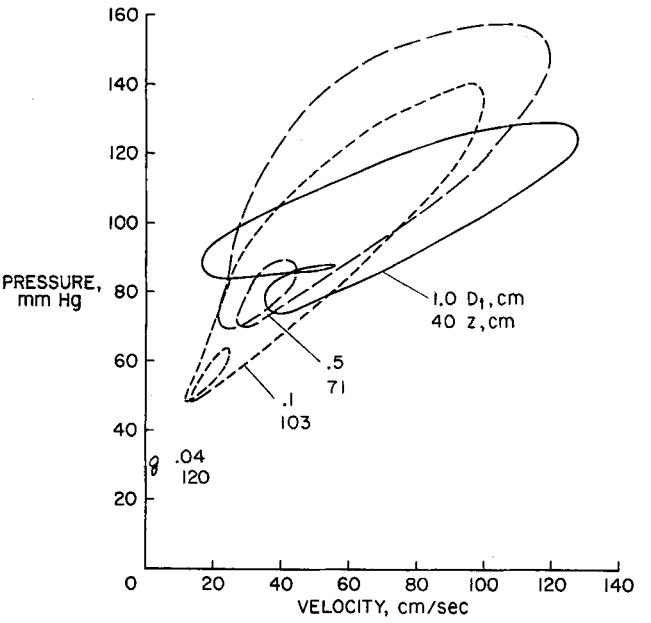

Figure 19
Pressure-velocity relation for the Standard Case at four different distances from the heart. D_t denotes the diameter of the artery at the indicated value of z where we examine the feasibility of using the peripheral resistance concept as a boundary condition. Each of the four closed curves represents the variation of pressure and flow during a full cardiac cycle. If the peripheral resistance concept were strictly valid, each of the four curves would be a straight line.

computed the pressure and flow pulses for four arteries with the same initial diameter, taper, $c(p, z)$, $\psi(p, z)$, ejection pattern and heart rate, but with different lengths, terminal diameters, and peripheral resistances. The values used for R_L are given in Table 2. In each case R_L was selected such as to yield at the root of the aorta the same diastolic pressure as does the Standard Case. The corresponding results are illustrated in Figures 20 and 21.

Table 2
Peripheral resistance for different terminal diameters

Diameter cm	Length cm	R_L dyne sec/cm^5
.04	120	2.39×10^6
.1	103	3.82×10^5
.5	71	9.93×10^3
1.0	40	2.60×10^3

The pressure and flow velocity profiles for the cases with terminal diameters of 0.04 cm and 0.1 cm cannot be distinguished within drawing accuracy from those for the Standard Case. Hence, for the mathematical model used here, the concept of peripheral resistance appears to be a very good approximation for arteries with end diameters of 0.1 cm or less.

For a terminal diameter of 0.5 cm the agreement is not as good. In this case we have deviations up to 4 mm Hg in pressure and up to 12 cm/sec in velocity. When the terminal diameter is taken as 1.0 cm at $L = 40$ cm, we note that extra waves begin to

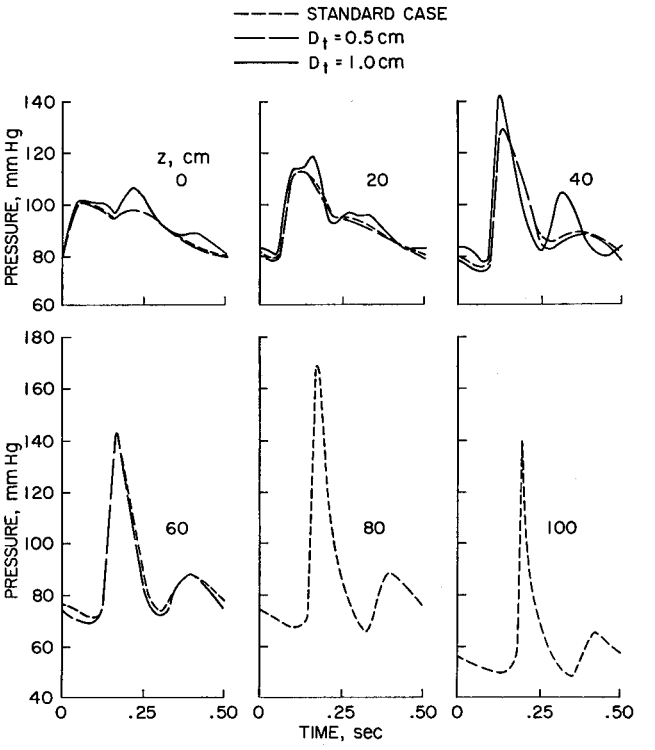

Figure 20
Pressure-time profiles obtained by specifying a peripheral resistance relation for different terminal diameters. The taper of the artery and other parameter values are the same as for the Standard Case.

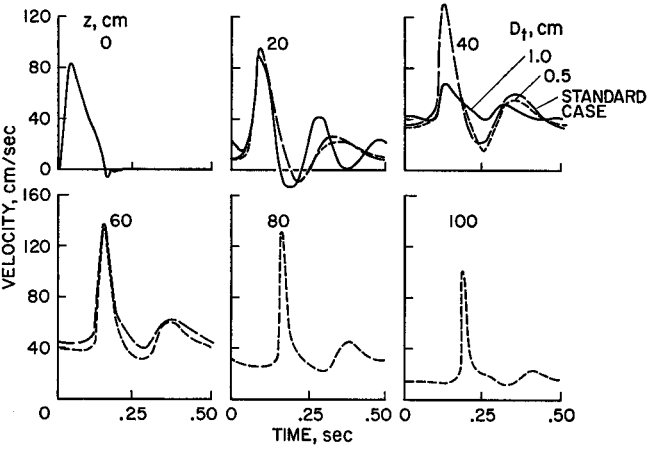

Figure 21
Velocity-time profiles corresponding to the pressure patterns shown in Figure 20, obtained by specifying a peripheral resistance relation at the distal end of the artery.

appear; the pressure and flow pulses are distorted and their magnitudes altered considerably. The peripheral resistance concept leads to results which can no longer be considered as acceptable approximations.

5. *Wave Front Velocity*

It has been shown that the familiar features of the natural pulse generated by the heart are predicted by the present model. The wave front velocity offers another comparison between theory and experiment. To define a characteristic point of the wave front on which to base the calculations of the velocity from the transmission time over a given distance, a straight line was drawn tangent to the front of the pressure pulse at the location of maximum slope (inflection point). Another line was drawn tangent to the pressure curve at the end of diastole preceding the beginning of the pulse. The intersection of these two lines was used as the characteristic point, whose speed is interpreted as the wave front velocity. The results for the pressure pulse of the Standard Case are shown in Figure 22.

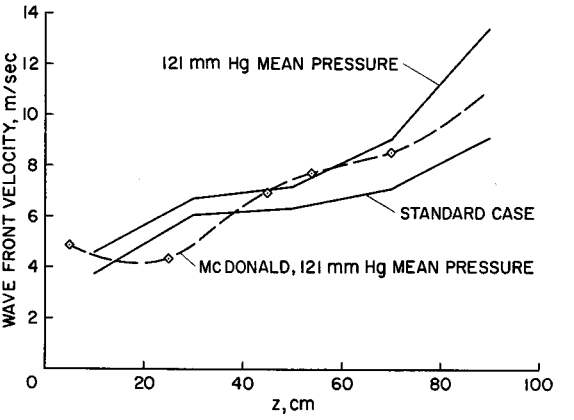

Figure 22
Wave front velocity of the pressure pulse as a function of distance from the aortic valve for the Standard Case (mean pressure = 88 mm Hg) and for a mean pressure of 121 mm Hg. Included for comparison is a curve extracted from Reference [7].

McDonald [7] has published some data on the wave front velocities for a situation where the mean pressure was 121 mm Hg. After scaling his distances to correspond to the hypothetical dog considered here, those velocities are also given in Figure 22. The comparison of McDonald's values with the results from the Standard Case is generally satisfactory. However such a comparison is not strictly proper because the mean pressure of the Standard Case is only 88 mm Hg. Therefore, an additional computer run was made using the parameters of the Standard Case except that the mean pressure was raised to 121 mm Hg by decreasing the outflow constant γ. The larger wave speeds due to the higher pressures should naturally cause larger values of the wave front velocity and the computer results, also given in Figure 22, confirm this. Further, recent measurements taken in the canine ascending aorta [33, 34] indicate that the wave front velocity averages 3.3 m/sec at pressures of 100 to 110 mm Hg. Assuming that a value of $z \simeq 5$ cm characterizes the region of the ascending aorta, we see that this data point also agrees with the computer results given in Figure 22.

It seems that our mathematical model of the aorta can be used to predict actual wave front velocities with reasonable accuracy. Of course, it would be more meaningful to compute the wave front velocities on the basis of the physical and geometric parameters of a particular dog, and then compare these velocities with the corresponding measurements made on the same dog.

References

[1] E. WETTERER and TH. KENNER, *Grundlagen der Dynamik des Arterienpulses*, (Springer-Verlag, Berlin 1968).

[2] D. A. MCDONALD, *Blood Flow in Arteries*, (Edward Arnold, Ltd., London 1960).

[3] P. A. PERONNEAU and F. LEGER, *Doppler Ultrasonic Pulsed Blood Flowmeter*, Proc. of the 8th Internat. Conf. on Medical and Biological Engineering, Chicago, Illinois, 1969.

[4] D. W. BAKER and D. E. STRANDNESS, *Instrumentation for the Early Detection of Arterial Occlusive Disease*, Proc. of the 8th Internat. Conf. on Medical and Biological Engineering, Chicago, Illinois, 1969.

[5] J. O. ARNDT, *Über die Mechanik der intakten A. carotis communis des Menschen unter verschiedenen Kreislaufbedingungen*, Arch. Kreislaufforsch. *59*, 153 (1969).

[6] M. ANLIKER, M. B. HISTAND and E. OGDEN, *Dispersion and Attenuation of Small Artificial Pressure Waves in the Canine Aorta*, Circulation Res. *23*, 539 (1968).

[7] D. A. MCDONALD, *Regional Pulse-Wave Velocity in the Arterial Tree*, J. Appl. Physiol. *24*, 73 (1968).

[8] M. ANLIKER, W. E. MORITZ and E. OGDEN, *Transmission Characteristics of Axial Waves in Blood Vessels*, J. Biomech. *1*, 235 (1968).

[9] *Physiology in the Space Environment, I. Circulation*, NAS-NRC Publ. 1485A, Nat. Acad. Sci.-Nat. Res. Council, Washington, D.C., 1968.

[10] J. R. WOMERSLEY, *An Elastic Tube Theory of Pulse Transmission and Oscillatory Flow in Mammalian Arteries*, WADC Tech. Report TR 56-614, Defense Decumentation Center, 1957.

[11] R. SKALAK, *Wave Propagation in Blood Flow*, In: *Biomechanics Symposium*, edited by Y. C. FUNG, New York, ASME, Appl. Mech. Div., 1966, p. 20–46.

[12] G. RUDINGER, *Review of Current Mathematical Methods for the Analysis of Blood Flow*, In: *Biomedical Fluid Mechanics Symposium*, New York, ASME, 1966, p. 1–33.

[13] J. W. LAMBERT, *On the Nonlinearities of Fluid Flow in Nonrigid Tubes*, J. Franklin Inst. *266*, 83 (1958).

[14] V. L. STREETER, W. F. KEITZER and D. F. BOHR, *Pulsatile Pressure and Flow Through Distensible Vessels*, Circulation Res. *13*, 3 (1963).

[15] G. RUDINGER, *Shock Waves in Mathematical Models of the Aorta*, J. Appl. Mech. (ASME Series E) *37*, 34 (1970).

[16] A. C. L. BARNARD, W. A. HUNT, W. P. TIMLAKE and E. VARLEY, *A Theory of Fluid Flow in Compliant Tubes*, Biophys. J. *6*, 717 (1966).

[17] A. C. L. BARNARD, W. A. HUNT, W. P. TIMLAKE and E. VARLEY, *Peaking of the Pressure Pulse in Fluid-Filled Tubes of Spatially Varying Compliance*, Biophys. J. *6*, 735 (1966).

[18] R. T. JONES, *Blood Flow*, Ann. Rev. Fluid Mech. *1*, 223 (1969).

[19] M. ANLIKER, M. K. WELLS and E. OGDEN, *The Transmission Characteristics of Large and Small Pressure Waves in the Abdominal Vena Cava*, IEEE Transactions on Bio-Medical Engineering *BME-16*, 262 (1969).

[20] R. L. LANGE and H. H. HECHT, *Genesis of Pistol Shot and Korotkoff Sounds*, Circulation *18*, 975 (1958).

[21] T. C. RUCH and H. D. PATTON, *Physiology and Biophysics*, (Saunders Co., Philadelphia 1965).

[22] H. N. HULTGREN, *Venous Pistol Shot Sounds*, Am. J. Cardiol. *10*, 667 (1962).

[23] M. B. HISTAND, *An Experimental Study of the Transmission Characteristics of Pressure Waves in the Aorta*, Ph. D. Dissertation, SUDAAR Report No. 369, Department of Aeronautics and Astronautics, Stanford University, California, 1969.

[24] D. J. PATEL, F. M. DEFREITAS, J. C. GREENFIELD, JR. and D. L. FRY, *Relationship of Radius to Pressure Along the Aorta in Living Dogs*, J. appl. Physiol. *18*, 1111 (1963).

[25] E. O. ATTINGER, H. SUGAWA, A. NAVARRO, A. RICCETTO and R. MARTIN, *Pressure-Flow Relations in Dog Arteries*, Circulation Res. *19*, 230 (1966).

[26] L. A. SAPIRSTEIN, *Regional Blood Flow by Fractional Distribution of Indicators*, Am. J. Physiol. *193*, 161 (1958).

[27] M. F. O'ROURKE, *Pressure and Flow in Arteries*, M. D. Thesis, University of Sydney, 1965.

[28] M. P. SPENCER and A. B. DENISON, *Pulsatile Blood Flow in the Vascular System*, In: *Handbook of Physiology, sect. 2, Circulation, Vol. II*, Washington, D.C., 1963, p. 839–864.

[29] M. LISTER, *The Numerical Solution of Hyperbolic Differential Equations by the Method of Characteristics*, In: *Mathematics for Digital Computers* (John Wiley and Sons, New York 1960).
[30] H. C. WIGGERS, *Cardiac Output and Total Peripheral Resistance Measurements in Experimental Dogs*, Am. J. Physiol. *140*, 519 (1944).
[31] E. JONES, M. ANLIKER and I. D. CHANG, *Effects of Viscosity and Constraints on the Dispersion and Dissipation of Waves in Large Blood Vessels*, Part I: *Theoretical Analysis*, Part II: *Comparison of Analysis with Experiments*, to be published in Biophysical Journal.
[32] R. T. JONES, *Simple Correction of the Windkessel Theory for the Dynamic Impedance of the Aorta*, Proc. of the 8th Internat. Conf. on Medical and Biological Engineering, Chicago, Illinois, 1969.
[33] W. W. NICHOLS, J. E. WEBSTER and D. A. MCDONALD, *Pulse Wave Velocity in the Ascending Aorta of the Dog*, Amer. Physiol. Soc. Proc., Davis, California, 1969.
[34] D. A. MCDONALD, *Frequency Dependence of Vascular Impedance*, In: *Pulsatile Blood Flow*, edited by E. O. ATTINGER (McGraw-Hill Book, Co., New York 1964), p. 115–133.
[35] W. SCHLIMMER, *Untersuchungen zu Elastizitätsproblemen der Aorta*, (Statistical Correlation of Pulse Wave Velocity with Age, Sex and Blood Pressure), Archiv für Kreislaufforsch. *47*, 189 (1965).
[36] T. J. REGAN, V. DEFAZIO, K. BINAK and H. K. HELLEMS, *Norepinephrine Induced Pulmonary Congestion in Patients with Aortic Valve Regurgitation*, J. Clin. Invest. *38*, 1564 (1959).
[37] C. K. FRIEDBERG, *Diseases of the Heart* (W. B. Saunders Co., Philadelphia 1955).
[38] D. A. MCDONALD, W. W. NICHOLS and N. T. KOUCHOUKOS, *Methods for Monitoring Cardiac Output*, Proc. of the Annual Conf. on Engineering in Medicine and Biology, Houston, Texas, 1968.

Zusammenfassung

Druck- und Strompulse mit grosser Amplitude erzeugt in der Aorta und in andern Hauptarterien des Hundes werden theoretisch berechnet für vorgeschriebene Ausströmungspulse von der linken Herzkammer und für gegebene physikalische und geometrische Eigenschaften des Kreislaufsystems. Der Blutausfluss durch die Äste und Verzweigungen der uns interessierenden arteriellen Leitung ist durch ein kontinuierlich verteiltes, von Druck und Ort abhängiges Ausflussmodell nachgeahmt. Am herzfernen Ende der Leitung ist als Randbedingung entweder der periphere Widerstand oder ein konstanter Druck vorgeschrieben. Die Geometrie der Leitung ist durch ihren kreisförmigen Querschnitt und den mit Herzdistanz exponentiell abnehmenden Radius definiert. Die elastischen Eigenschaften der Gefässwand sind durch die von Ort und Druck abhängige Geschwindigkeit kleiner Druckwellen gegeben. Durch Integration der Beziehung zwischen Wellengeschwindigkeit und Querschnittsdehnung ist damit auch der Querschnitt als Funktion des Druckes und der Herzdistanz vorgeschrieben. Die nichtlinearen Gleichungen für eindimensionale Strömung einer inkompressibler Flüssigkeit werden mit Hilfe der Charakteristikenmethode integriert für Kreislaufparameterwerte die einem hypothetischen Hund von 30 kg Gewicht entsprechen. Das verwendete mathematische Modell für die arterielle Leitung wiedergibt manche der bekannten Eigenschaften des vom Herzen erzeugten Pulses, einschliesslich die Klappenincisur, das Ansteigen und Abfallen der Höhe des systolischen Druckgipfels mit wachsender Entfernung vom Herzen. Während der Fortpflanzung der Pulswelle zeichnet sich eine zunehmende Steilheit der Wellenfront ab, die jedoch nicht merkbar ist wenn man die grundlegenden Gleichungen linearisiert. Die numerischen Ergebnisse weisen darauf hin, dass die sekundäre (dicrotic) Welle durch Reflexionen erzeugt wird, und als solche von der Verjüngung des Querschnittes und vom Blutausfluss abhängt.

(Received: June 8, 1970)